LBL-24776
Preprint

Lawrence Berkeley Laboratory
UNIVERSITY OF CALIFORNIA

Engineering Division

Submitted to Nuclear Instruments and Methods
in Physics Research A

Low Noise Germanium Radial Drift Detector

P.N. Luke

February 1988

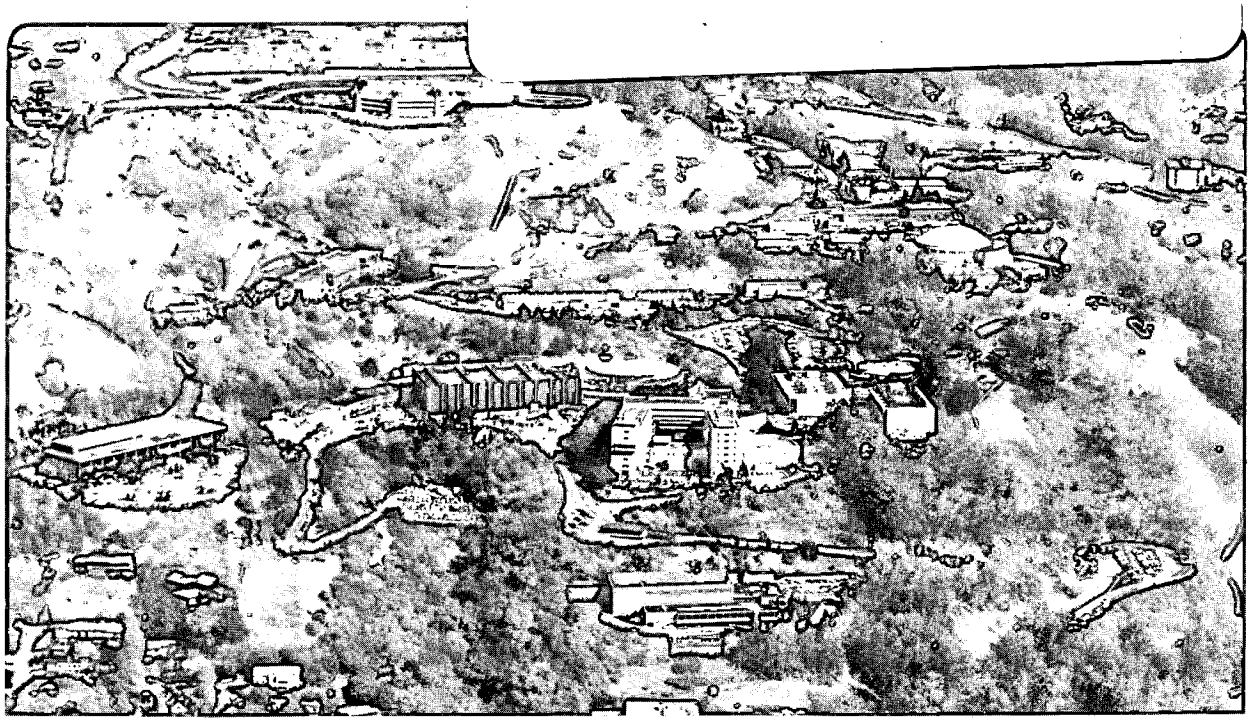

Prepared for the U.S. Department of Energy under Contract DE-AC03-76SF00098

DISCLAIMER

LOW NOISE GERMANIUM RADIAL DRIFT DETECTOR

Paul N. Luke
Electronics Engineering Office
Lawrence Berkeley Laboratory
University of California
Berkeley, CA 94720

Abstract

A germanium radial drift detector with a built-in drift field has been fabricated using conventional processing techniques. It has an active area of 5 cm^2 and a full depletion capacitance of 1.4 pf. It exhibited low noise and good energy resolution. Detector pulse shapes have been measured and found to agree well with the calculated shape.

1. Introduction

The idea of the semiconductor drift detector was first developed by Gatti and Rehak several years ago[1]. These detectors have a planar p^+-n-p^+ structure (for the case of n-type material) with a small area n^+ contact off to one side. By applying a reverse voltage across the n^+ and p^+ contacts, the bulk can be depleted. At full depletion, a potential valley parallel to the plane of the detector is established within the device. As electrons and holes are created by incoming radiations, the holes will drift to the p^+ contact and be collected while the electrons drift to the mid-plane of the detector. To collect the electrons, a drift field is required to transport them to the n^+ contact. This can be accomplished by segmenting the p^+ contact and applying external potentials to them. Position information can thus be obtained by measuring the drift time of the electrons. Another important feature of the semiconductor drift detectors is their low capacitances, which make them useful as large area, low noise detectors.

Based on this device concept, many experimental silicon drift detectors has been fabricated and additional new devices have been proposed.[2] However, the need for contact segmentation and externally applied potentials to create the drift field create complications in implementing these devices especially for other semiconductors for which there is no well-established planar processing technology. To avoid these complications, detectors with a built-in drift field can be used. A built-in drift field can be generated either by using materials with an impurity concentration gradient or using a tapered detector structure. Both approaches have been explored and applied to germanium detectors.[3,4] These detectors have the additional advantage that they present a continuous thin window to incoming radiations. These earlier devices were used as position-sensitive detectors. The low drift field and long drift distances in these detectors resulted in significant trapping effects.[3] For non-position-sensitive applications where only the low capacitances of the drift detectors are of interest, the drift field can be increased to minimize trapping effects. Also, by using a radial drift geometry, both the drift distance and the capacitance can be minimized for a certain detector area.

To obtain a built-in drift field in a radial drift detector, one could use material with a radial impurity gradient. Although it may be possible to produce such material, this is considered impractical. With a tapered geometry, readily available material with constant impurity concentrations can be used.

2. Principle of operation

The geometry of a tapered radial drift detector is depicted in Fig. 1 which shows one half of the cross-sectional view. The device can be

visualized as a solid of revolution about the z-axis. As one increased the reverse bias applied between the p^+ and n^+ contacts, the width of the depletion layer formed at the p^+-n junction on both sides of the detector will increase. Depletion of the full local thickness will occur first at the rim of the device, and with further increase in bias voltage, the undepleted layer at the middle will shrink towards the n^+ contact until full depletion is reached. The potential inside the device at full depletion is shown in Fig. 2. A potential valley with increasing depth is formed. As electron-hole pairs are generated by incoming radiations, the holes will drift to the p^+ contact and the electrons will drift toward the mid plane of the device and then drift radially inward to the n^+ contact.

For this device geometry, the Poisson's equation cannot be solved in closed form. The potential inside the device as shown in Fig. 2 was calculated using the finite difference method performed on a personal computer. However, for a device with a shallow taper, as is the case here, the magnitude of the radial drift field can be easily estimated without calculating the full potential. Since the depth of the potential well at a certain radial distance is just the potential required to deplete half the local thickness of the device, the radial drift field can be written as,

$$E_d(r) = - \frac{eN}{4\varepsilon} k(L_o - kr)$$

where $L(r) = L_o - kr$ is the local thickness of the detector, N is the net electrically active impurity concentration, e is the electronic charge and ε is the permittivity.

3. Test device

A test device with the basic structure shown in Fig. 1 has been fabricated. It has a diameter of 27 mm and a thickness that ranged from 3 mm

near the center to 1 mm at the rim. The n^+ contact was formed by lithium diffusion and the p^+ contact was formed by boron ion implantation. N-type germanium with a net impurity concentration of 3×10^{11} cm^{-3} was used. The resultant radial drift field along the mid-plane of the device ranged from ~ 180 V/cm near the rim to ~ 450 V/cm near the n^+ contact. This drift field is substantially higher than those of the previous germanium drift detectors. The detector was operated at near liquid nitrogen temperature.

Figure 3 shows the capacitance-voltage characteristics of the detector. At low biases, a layer of undepleted material exists along the mid-plane of the detector resulting in the high capacitance. As full depletion is reached first near the rim of the detector and then towards the center, the capacitance drops rapidly and then levels off at a low value of 1.4 pf, corresponding to full depletion of the detector.

The low capacitance of the detector resulted in low electronic noise and the higher drift field greatly improves the charge collection efficiency of the device compared to the previous germanium drift detectors.[3] Figure 4 shows spectra taken with the radial drift detector using a pulse-opto reset amplifier. The full area of the detector was illuminated except for an approximately 1 mm wide support area at the rim. As can be seen, there is no significant trapping effects for photon energy up to 60 keV. At low photon energies, the resolution is limited by electronic noise. While the measured electronic noise of 120 eV at 17 μs peaking time is commonly achieved with small area detectors, it is obtained here for a detector with an active area of 5 cm^2. In comparison, standard planar detectors with similar active area and thickness would have a capacitance of tens of pf and electronic noise in the several hundred eV range. Another important feature of the radial drift detector is that its active area can be increased without increasing its capacitance.

4. Pulse shape

In a drift detector, collection times for signal carriers can be quite long, depending on the drift field and the drift distances. However, the rise time of the main part of the signal can still be relatively short. This is due to the shielding effect of the outer electrode and is further aided in this case by the radial geometry of the device. In general, the instantaneous current induced at an electrode of a detector due to the movement of a point charge (q) can be calculated as follows:[5]

$$i = q \vec{v}(E) \cdot \vec{E}_o$$

where $\vec{v}(E)$ is the velocity of the point charge, E_o is the hypothethical electric field that would exist inside the device under the conditions of zero space charge and unit electric potential at the subject electrode with all other electrodes at zero potential. Note that E_o is generally not related to the actual electric field (E) inside the device. The actual field comes in only in its effect on the velocity of the signal charge. Since, in the case of the radial drift detector, E_o decreases rapidly away from the central electrode, very little signal is induced by the drifting carriers until they are making the final approach to the center electrode.

Figure 5 shows the calculated charge pulse obtained by releasing a point charge (q) at the rim of the detector and allowing it to drift along the mid-plane of the detector to the center electrode. While the total collection time is over 200 ns, almost all of the signal is induced during the last 70 ns which corresponds to the last 4 mm of the drift path. As a result, single events such as those that are due to photoelectric interactions occurring in most of the detector volume will produce effectively similar pulse shapes with different delay times. This is demonstrated in Fig. 6 which shows actual wide band signals obtained from the radial drift detector under full area

illumination of 60 keV photons from an Am^{241} source. The exposure is taken over many pulses with the oscilloscope triggered internally by the initial rise of the pulses. The pulse shape agrees well with the calculated shape and uniformity of the pulses is evident. In the present case, the rise time contribution due to the spreading of the charge cloud as a result of dispersion in a non-uniform drift field, charge diffusion, and mutual repulsion of the signal carriers[5] is estimated to be less than 5 ns. This implies that substantially faster rise time is possible and can be acheived by reducing the size of the center electrode which would make E_o a more sharply peaked function.

5. Conclusion

In summary, a germanium radial drift detector with a built-in drift field has been fabricated using conventional processing techniques. It has a low full-depletion capacitance and exibited low noise and good energy resolution. These characteristics make it an interesting detector to consider for low energy gamma-ray or x-ray spectroscopy applications requiring large active areas. The uniformity of its pulse shape and the fast rise time that can be achieved may also be advantageous in high rate applications. Such a device can also be used as a low-noise near-infrared photodetector.

Acknowledgments

We would like to thank F. S. Goulding and R. H. Pehl for their support and interest. This work was supported by the Director's Office of Energy Research, Office of Health and Environmental Research, Pollutant Characterization and Safety Research Division of the U.S. Department of Energy under Contract No. DE-AC03-76SF00098.

References

[1] E. Gatti and P. Rehak, Nucl. Instr. and Meth. 225 (1984) 608.

[2] J. Kemmer and G. Lutz, Nucl. Instr. and Meth. A253 (1987) 365.

[3] P.N. Luke, N.W. Madden and F.S. Goulding, IEEE Trans. Nucl. Sci. NS-32, No.1 (1985) 457.

[4] P.N. Luke and E.E. Haller, J. Appl. Phys. 59 (1986) 3734.

[5] P.A. Tove and K. Falk, Nucl. Instr. and Meth. 29 (1964) 66.

Figure captions

Fig. 1 Structure of the radial drift detector (half cross-sectional view).

Fig. 2 Electric potential inside the detector at full depletion.

Fig. 3 Capacitance vs. voltage of the test device.

Fig. 4 (a) Fe^{55} and (b) Am^{241} spectra taken with an amplifier peaking time of 17 μs.

Fig. 5 Calculated charge pulse due to a point charge released at the rim of the detector.

Fig. 6 Oscilloscope traces of detector charge pulses from an Am^{241} source. Horizontal axis: 50 ns/div.

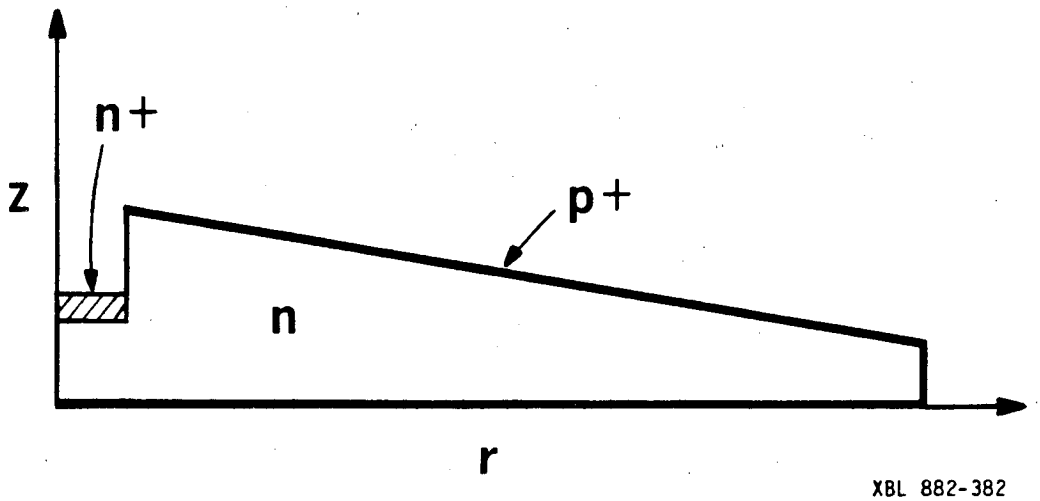

Fig. 1.

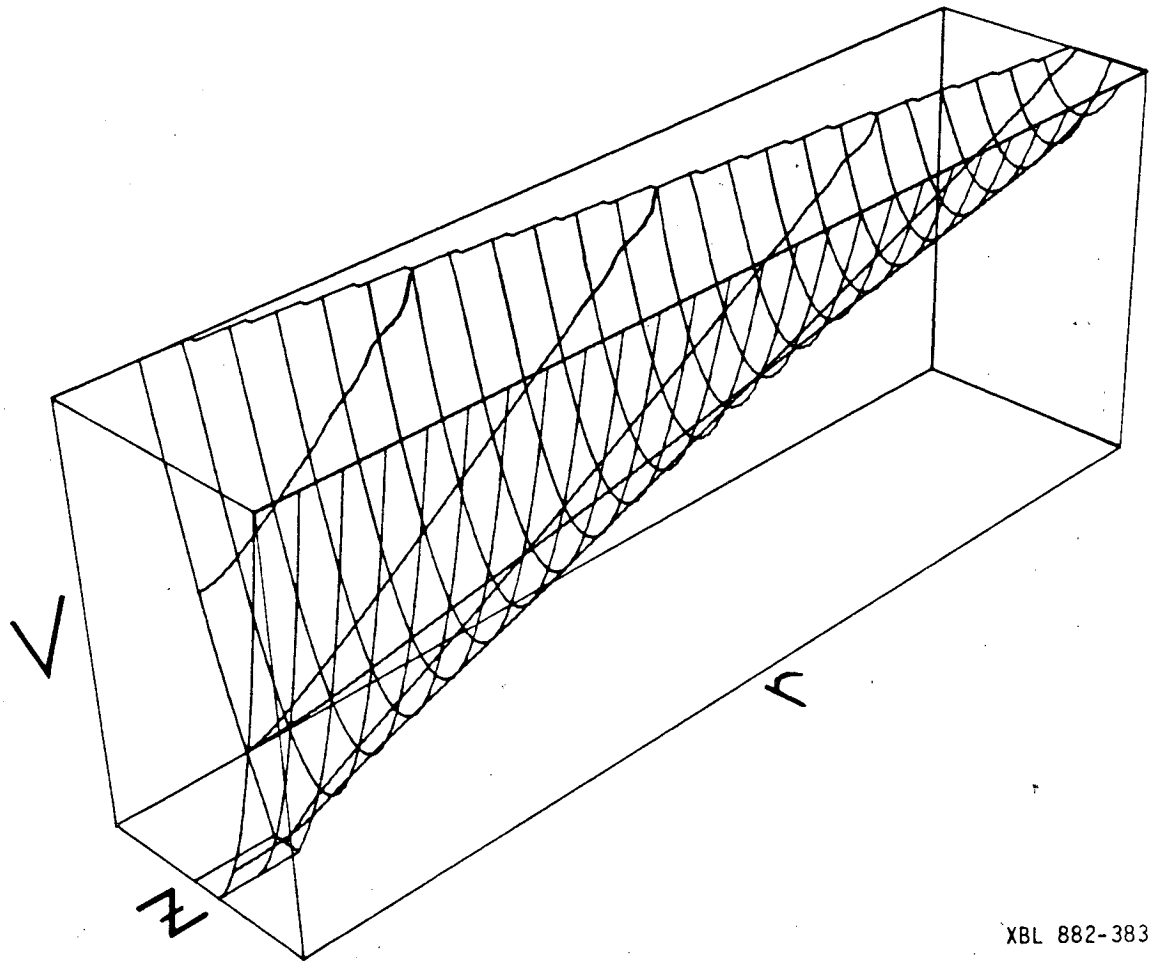

XBL 882-383

Fig. 2.

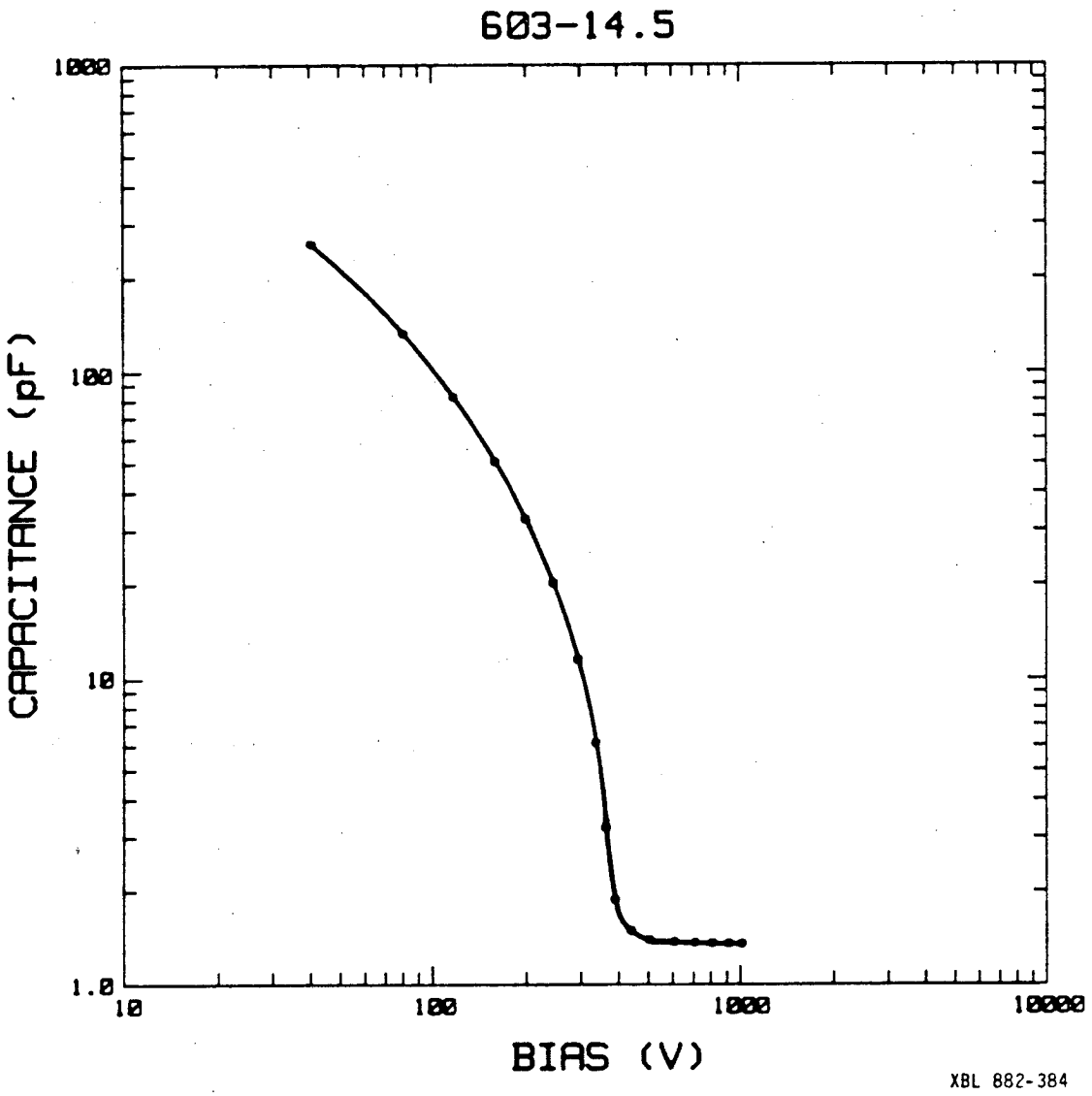
603-14.5
1000
100
10
1.0
CAPACITANCE (pF)
10
100
1000
10000
BIAS (V)
XBL 882-384

Fig. 3.

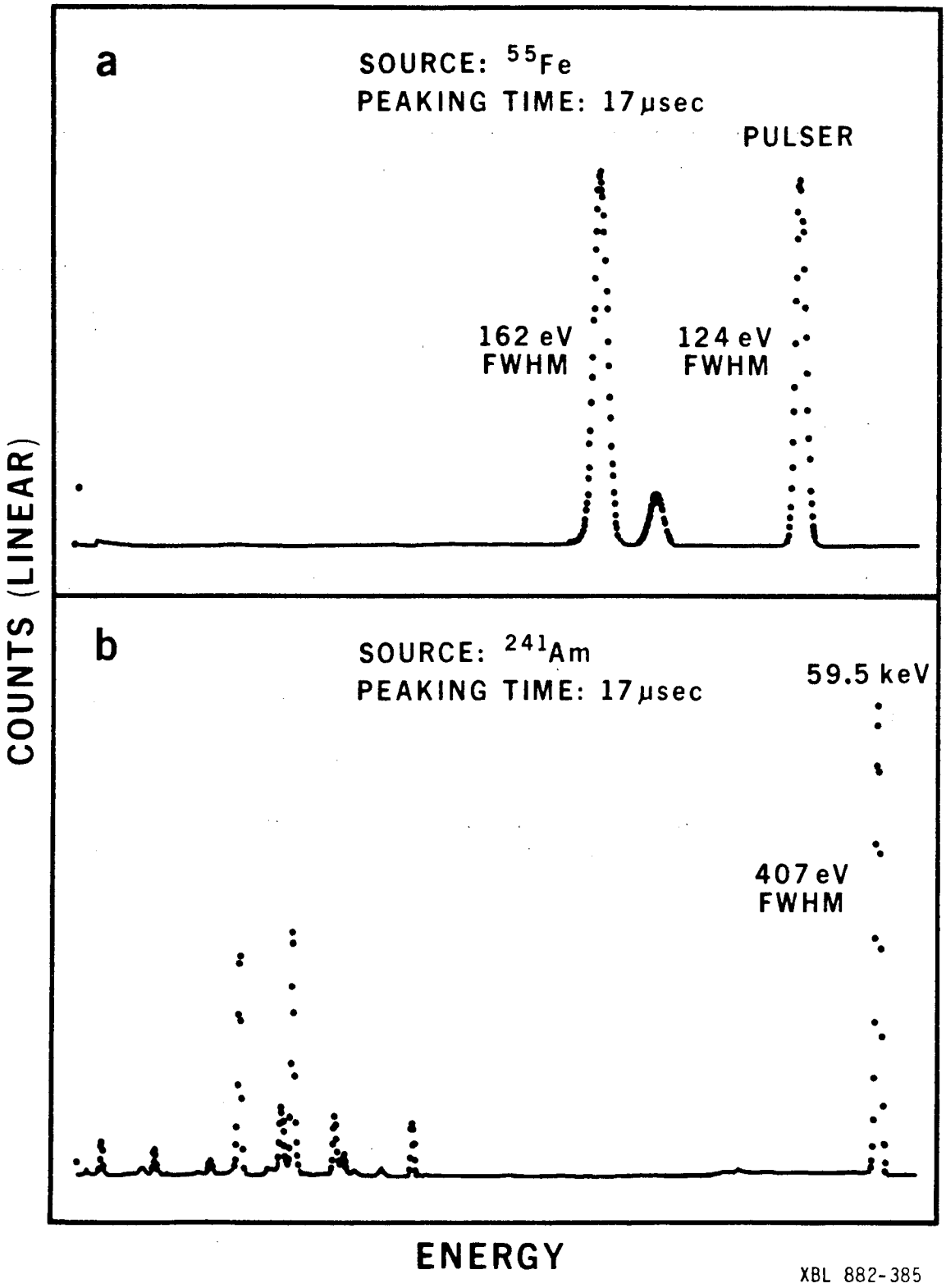
a
SOURCE: ^{55}Fe
PEAKING TIME: 17 μsec
PULSER
162 eV
FWHM
124 eV
FWHM
b
SOURCE: ^{241}Am
PEAKING TIME: 17 μsec
59.5 keV
407 eV
FWHM
COUNTS (LINEAR)
ENERGY
XBL 882-385

Fig. 4.

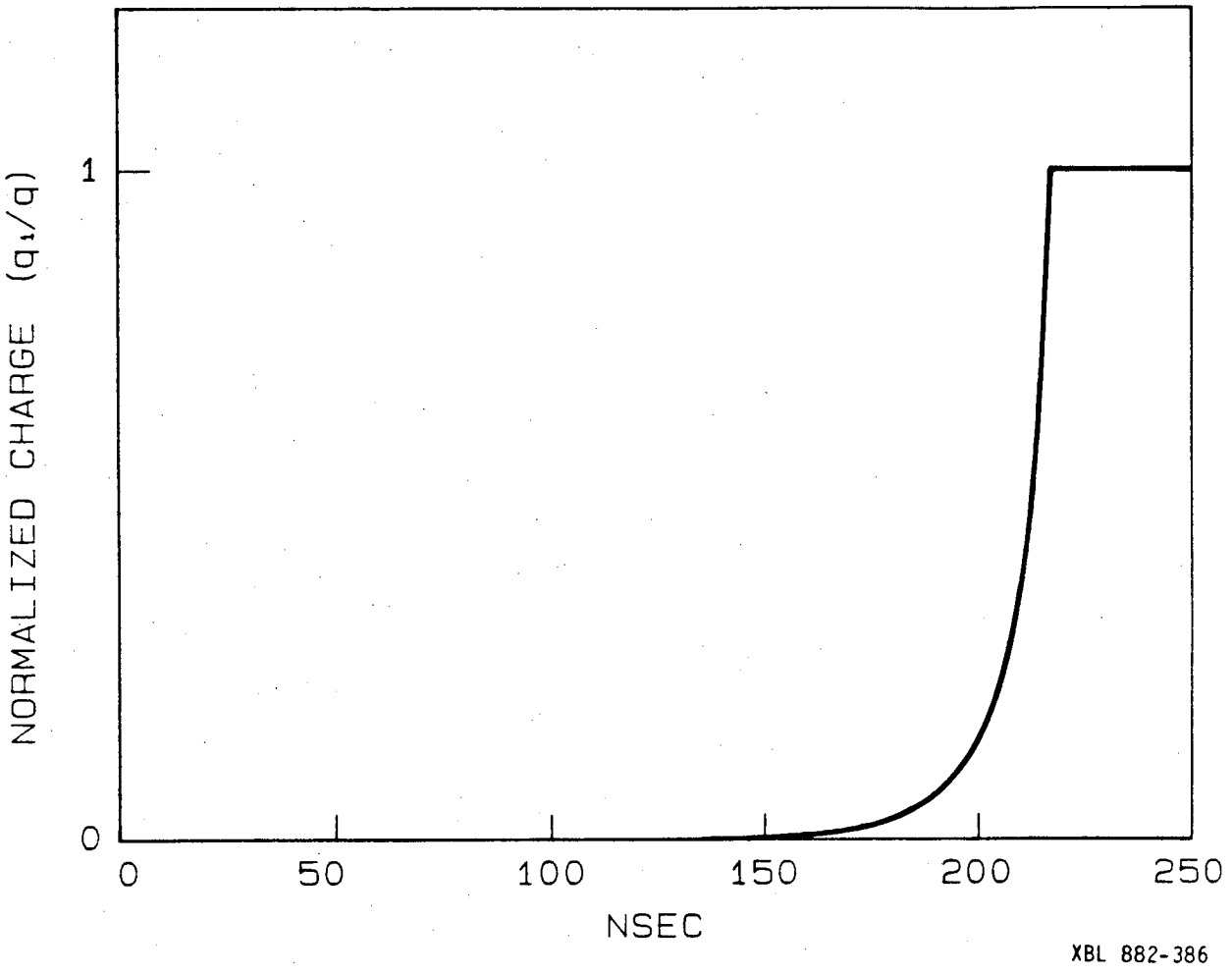

Fig. 5.

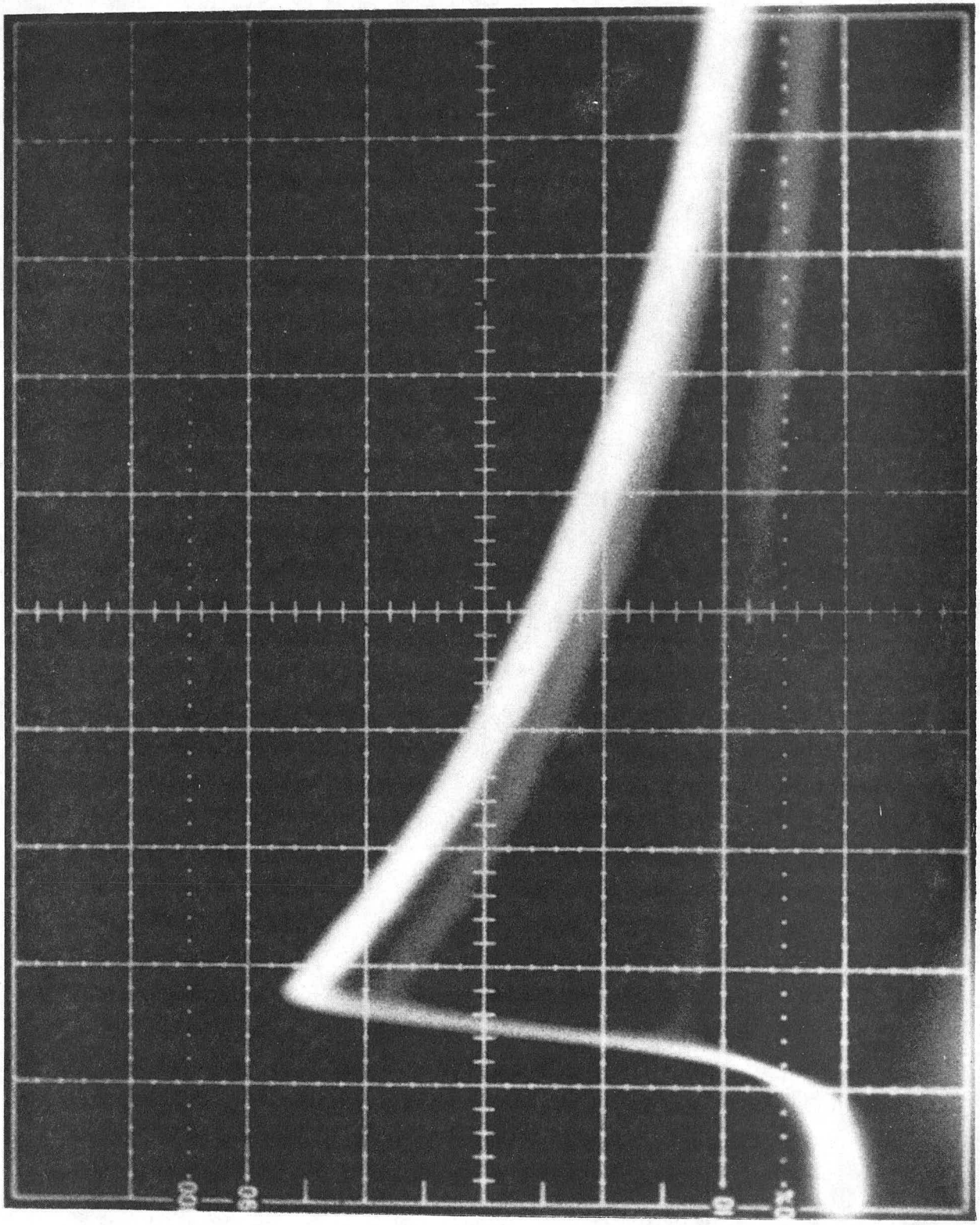

XBB 882-844

Fig. 6

LAWRENCE BERKELEY LABORATORY
TECHNICAL INFORMATION DEPARTMENT
UNIVERSITY OF CALIFORNIA
BERKELEY, CALIFORNIA 94720